Formation of saucer-shaped sills

A. MALTHE-SØRENSSEN[1], S. PLANKE[2], H. SVENSEN[1] & B. JAMTVEIT[1]
[1]*Physics of Geological Processes, Department of Physics, University of Oslo, Box 1048 Blindern, N-0316 Oslo, Norway (e-mail: malthe@fys.uio.no)*
[2]*Volcanic Basin Petroleum Research AS, Forskningsparken, Gaustadalleen 21, N-0349 Oslo, Norway*

Abstract: We have developed a coupled model for sill emplacement in sedimentary basins. The intruded sedimentary strata are approximated as an elastic material modelled using a discrete element method. A non-viscous fluid is used to approximate the intruding magmatic sill. The model has been used to study quasi-static sill emplacement in simple basin geometries. The simulations show that saucer-shaped sill complexes are formed in the simplest basin configurations defined as having homogeneous infill and initial isotropic stress conditions. Anisotropic stress fields are formed around the sill tips during the emplacement due to uplift of the overburden. The introduction of this stress asymmetry leads to the formation of transgressive sill segments when the length of the horizontal segment exceeds two to three times the overburden thickness. New field and seismic observations corroborate the results obtained from the modelling. Recent fieldwork in undeformed parts of the Karoo Basin, South Africa, shows that saucer-shaped sills are common in the middle and upper parts of the basin. Similar saucer shaped sill complexes are also mapped on new two- and three-dimensional seismic data offshore of Mid-Norway and on the NW Australian shelf, whereas planar and segmented sheet intrusions are more common in structured and deep basin provinces.

The emplacement of magmatic sills in sedimentary basins has major implications on the development and structure of the basins. The introduction of hot melt into the sedimentary sequence will cause heating, expulsion of pore fluids, and associated metamorphic reactions. The solidified and cold sills will subsequently influence the basin rheology, strength, and permeability structure. These magmatic processes will also influence the petroleum prospectivity through enhanced maturation, and formation of migration pathways (Schutter 2003).

Sheet intrusions, such as dykes, sills, and laccoliths, are important for rapid magma transport in the Earth's crust (e.g. Rubin 1995). Dykes are near-vertical magma-filled fractures driven primarily by the buoyancy of hot magma. Sills are dominantly layer-parallel sheets with transgressive segments. An impressive Jurassic sill complex is found in the Karoo Basin, South Africa, including extensive saucer-shaped sills (e.g. Du Toit 1920; Bradley 1965; Chevallier & Woodford 1999). A review of sill geometries and emplacement mechanisms is given by Francis (1982). Laccoliths are layer-parallel intrusions with a flat bottom and a dome-shaped top. The term was introduced by Gilbert (1877) based on studies in the Henry Mountains, Utah. Laccoliths in the Henry Mountains and elsewhere in the North America have subsequently been studied by, for example, Johnson & Pollard (1973) and Corry (1988). Sill–sediment boundaries represent high-impedance contrasts, and sill complexes are therefore well imaged on seismic reflection data. Recently, a number of studies on the 2D and 3D geometries of sill complexes have been made, in particular along the volcanic margins of the NE Atlantic (Skogseid *et al.* 1992; Berndt *et al.* 2000; Smallwood & Maresh 2002).

The wide range of sill complex geometries found in the field and from seismic data has generally not been addressed in theoretical studies, which have concentrated on the 2D shape of single dykes or sills, mostly in two dimensions (Pollard & Johnson 1973; Lister & Kerr 1991). The main focus of this work has been on the flow of viscous magma and the interplay between the viscous fluid flow and fracturing. In particular, various models on the effects of viscous pressure-drop along the sill and the fracturing of fluid-filled cracks have been discussed (Lister & Kerr 1991). The limitations of linear elastic fracture mechanics in studies of the propagation of an individual dykes or sills have also been addressed (Rubin 1993; Khazan & Fialko 1995).

Various authors have addressed mechanisms responsible for the dyke to sill transition, but with few quantitative modelling results to

From: BREITKREUZ, C. & PETFORD, N. (eds) 2004. *Physical Geology of High-Level Magmatic Systems.* Geological Society, London, Special Publications, **234**, 215–227. 0305-8719/04/$15.00

support the ideas. The studies of laccolith and sill intrusions in the Henry Mountains (Johnson & Pollard 1973; Pollard & Johnson 1973) showed how linear elasticity theory could be applied to study the shape and development of sheet intrusions. Further theoretical studies of the interplay between structure, stress heterogeneities, and dyke and sill shapes (Pollard *et al.* 1975) have further shown that linear elasticity theory can bring important insights into dyke and sill emplacement without a full treatment of the effects of viscous magma or the detailed processes near the propagating dyke tip.

However, the advances in the study of flow in a single dyke have little significance for understanding the complex interaction between the intruding sill and the surrounding sediments, interactions between different sills, and the internal dynamics during emplacement. Effects such as magma-tectonism and inflation–deflation cycles have not previously been addressed by theoretical fluid-mechanical models.

In this paper, we focus on the interactions between sill emplacement and sediment deformation. We have developed a numerical model that can be used to study complexities of sill emplacement in heterogeneous materials. Our main emphasis here is to find the simplest possible model that contains only the essential physical processes needed to reproduce the most important phenomena observed without describing the whole process in detail.

Sill emplacement modelling

For dykes propagating upwards through the crust, the main driving forces are buoyancy, due to density difference between magma and host rock, and magma overpressure in the reservoir (Lister & Kerr 1991). It has been suggested that the injection of sills from dykes are driven by a pressure head due to the overshooting of dykes (Francis 1982), or that sills are fed laterally by dykes (Chevallier & Woodford 1999). In this article we will focus on the sill emplacement mechanism without considering how magma is supplied in detail. This is a reasonable assumption when studying several aspects of sill emplacement, such as the final sill geometry and tectonic effects of sill emplacment, in particular because these have proved very difficult if not impossible to infer the injection point of a sill complex based on geometries found in seismic data, or from field data. The focus is on providing the simplest possible model that contains the necessary mechanisms to provide an explanation for particular, observed characteristics of sill emplacement.

The sill emplacement is a coupled process where the flowing magma deforms and affects the surrounding matrix, and the deformation and fracturing of the matrix affects the flow of magma. A model of sill emplacement must take into account this fully coupled process: the magma should be represented by a fluid moving in a geometry determined by the deformation of the surrounding matrix, which will deform, and possibly change its material properties, due to the magma emplacement process.

We model this coupled process by representing the matrix as an elastic material and the magma as a fluid. The assumption of elasticity is reasonable at large length-scales and at shallow depths, that is at depths less than 5 km (Atkinson 1984). The elastic material can be represented by a discrete element model. Such models are well suited to study coupled processes, such as fracture-enhanced transport in eclogitization processes (Jamtveit *et al.* 2000) and hydro-fracturing processes (Flekkøy *et al.* 2002). Discrete element models also provide a simple, physical framework for studying dynamic fracture processes in which the surface geometry changes continuously during deformation. Discrete element models are also equally well suited for quantitative calculations, as other discretization approaches to continuum elasticity theory (Monette & Anderson 1994).

We initially make the assumption that the magma can be modelled as a non-viscous fluid with a constant pressure. This is a reasonable assumption for a slow deformation process, in which the viscous forces are small, and the rate of deformation due to magma injection is small compared to the time-scale of elastic equilibration in the host rock. It is also a reasonable assumption for a solidifying magma when the flow velocities are very small. The use of non-viscous fluid to model the magma implies that there is no pressure drop from the inlet along the length of the sill, and there are no shear forces on the boundaries. However, the actual thickness of a sill will depend on the viscosity, and therefore also on the rate of injection and the rate of solidification. Viscous effects are also important to understand the rate of emplacement, but may not be similarly important for modelling the shape of the sill or the deformation of the host rock during the emplacement. The effects of viscosity can, however, be studied in detail when the location of the injection point is known, and viscous effects can be approximated by a gradual change in the pressure in the sill away from the inlet.

Discrete element modelling

The sedimentary basin is modelled as a linear elastic material using a discrete element model

(DEM). The DEM model is a discrete realization of the linear elastic continuum formulation of the problem (Flekkøy *et al.* 2002). However, the DEM model deviates from the continuum formulation in the choice of boundary conditions. In the DEM approach, the elastic material is modelled as a network of elements – spheres – connected by elastic bonds in the form of springs or beams.

We have demonstrated that the equilibrium configuration of a triangular lattice of linear springs is equivalent to the equilibrium solution to the linear elasticity problem for an isotropic material (Flekkøy *et al.* 2002). Thus, as a first-order approach we have used a triangular lattice with springs to model the elastic sediments. The forces acting on a particle can be decomposed in an interaction force, f_i^n, due to inter-particle interactions, and interaction with boundaries, gravity, f_i^g, and external forces, f_i^e, such as the force transfer from the magma:

$$f_i^n = f_i^n + f_i^g + f_i^e. \tag{1}$$

For a network of springs, the force due to inter-particle interactions is:

$$\boldsymbol{f}_i^n = \sum_j k_{i,j}\left(\left(\left|\boldsymbol{x}_i - \boldsymbol{x}_j\right|\right) - l_{i,j}\right)\boldsymbol{u}_{i,j} \tag{2}$$

where the sum is over all connected neighbours j, $\boldsymbol{x}_j$ is the position of node j, $l_{i,j}$ is the equilibrium length for the connection between nodes i and j, and $\boldsymbol{u}_{i,j}$ is a unit vector pointing from the centre of node i to the centre of node j.

The spring constant $k_{i,j}$ may vary locally for a heterogeneous material. This corresponds to local variations in the Young's modulus for the material. Typically, we assume that the material has homogeneous elastic properties, that is, $k_{i,j} = k$. However, the method presented here can easily be extended to model heterogeneous elastic properties.

The gravitational term f_i^g describes the gravitational force on the particle. For a particle of mass density ρ_i, the gravitational force in a two-dimensional system is:

$$\boldsymbol{f}_i^g = \rho_i \pi r_i^2 w_z g \boldsymbol{u}_y \tag{3}$$

where r_i is the radius of particle i, and w_z is the thickness in the third dimension. The mass density for the particle is related to the mass density of the elastic material ρ_m through the porosity ϕ of the packing: $\rho_m(1-\phi) = \rho_i$.

The external force f_i^e, is due to the coupling of the elastic material to the magma flow. For the case of a non-viscous magma, the only coupling force is the pressure gradient, given by the pressure (P) in the magma. However, the method presented here is easily extended to include both normal and shear forces in viscous magma. The pressure force acts in the direction of the local surface normal, which is calculated from the local configuration of elements as illustrated in Figure 1. This results in a force:

$$\boldsymbol{f}_i^e = PA_i\boldsymbol{u}_i^P \tag{4}$$

where P is the local pressure in the magma, A_i represents the local surface area, and $\boldsymbol{u}_i^P$ is the local surface normal to the sill–matrix interface.

The magma pressure P includes the effect of hydrostatic pressure in the magma with a given magma density ρ_s, $P = P_0 + \rho_s g(h - y)$, where h and P_0 corresponds to the level of injection.

For a system with small displacements, that is, a system which is at the linear elastic limit, we need only consider deviations from the lithostatic pressure. In this model, the effect of gravity is included in a lithostatic term for the stresses, and the hydrostatic pressure term in the magma pressure depends only on the difference in densities: $P = P_0 + \Delta\rho g(h - y)$. This method is used for the calculations, and all illustrations display the calculated stresses minus the lithostatic pressure. However, the gravitational term will be included in the equations in order to illustrate its role in non-isotropic and non-homogeneous systems.

The equations should be non-dimensionalized in order to show how the simulation parameters relate to real-world parameters. We introduce the non-dimensional parameters: $x = x'l$ and $k_{i,j} = k'_{i,j}k$, where l is the length corresponding to a diameter of the simulation particle. The spring constant normalization factor k can be related to the Young's modulus of the material for a triangular lattice of nodes (Flekkøy *et al.* 2002):

$$k = \frac{\sqrt{3}}{2} E w_z \tag{5}$$

where $E = E_0 2/\sqrt{3}$ is the Young's modulus of the material, and w_z corresponds to the thickness of the two-dimensional sample used in the simulation. It can be demonstrated that the value of w_z does not have any significance for simulation parameters or stresses, and is only needed for dimensional consistency. The surface area is rescaled using both l and w_z: $A_i = w_z l A'_i$.

The resulting equation for the force on particle is thus:

$$\boldsymbol{f}_i = E_0 w l \left\{ \sum_j k'_{i,j}\left(\left|\vec{\boldsymbol{x}}'_i - \vec{\boldsymbol{x}}'_j\right| - l'_{i,j}\right)\vec{\boldsymbol{u}}_{i,j} \right. \tag{6}$$

$$\left. - \frac{\pi\rho \lg}{E_0}\left(r'_i\right)^2 \frac{\rho_i}{\rho}\vec{\boldsymbol{u}}_z + \frac{P}{E_0} A'_i \vec{\boldsymbol{u}}_i^P \right\} \tag{7}$$

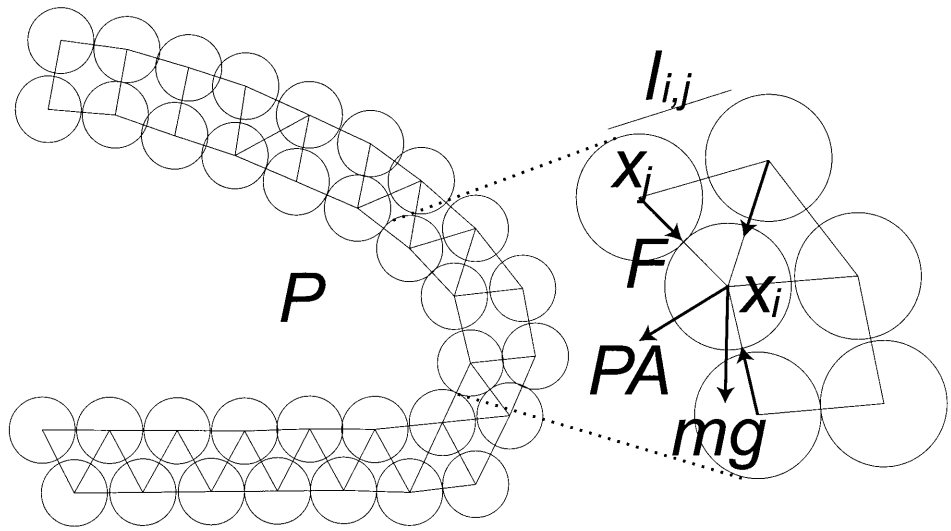

Fig. 1. Illustration of coupled DEM model for sill emplacement studies. The elastic material is modelled by a network of interconnected springs drawn as lines between the circular particles. The springs are initially placed on a triangular network. The sill is represented as a moving fracture, illustrated as the region without springs. A pressure P acts from the magma in the sill on the surrounding particles. The illustration on the right illustrates the forces acting on a particle i. The forces are: contact forces due to connections to other particles, calculated as a spring force proportional to the elongation of the springs; a gravitational force mg, and a pressure force PA_i, where A_i is the local surface area of the sill-magma boundary associated with particle i. For a given pressure P, the equilibrium configuration of the elastic network is found.

Simulations are performed in the non-dimensional co-ordinate system, and then scaled back to real-world quantities using the scaling relations. Stresses (σ'_{ij}) measured in simulation co-ordinates are rescaled to real co-ordinates according to $\sigma_{ij} = E_0\sigma'_{ij}$.

The equilibrium configuration for the system can be found by standard relaxation techniques. We have used a specially tailored method based on successive over-relaxations (Allen 1954). This method uses extra relaxations close to fracture tips, and is particularly efficient for fracturing systems, where most of the deformation occurs near fractures and fracture tips.

The system is constrained by elastic boundaries in the form of elastic walls. The wall is modelled as a linear spring, so that the force on a particle due to the wall interaction is proportional to the distance from the particle to the wall. For a particle in contact with a wall parallel to the x-axis at $y = y_w$, the force from the wall on particle i is:

$$\boldsymbol{f}_i = \begin{cases} k_w(y_i + r_i - y_w)\,\boldsymbol{u}_y & y_i + r_i - y_w > 0 \\ \mathbf{0} & y_i + r_i - y_w \leq 0 \end{cases} \quad (8)$$

where r_i is the radius of particle i, and $\boldsymbol{u}_y$ is a unit vector along the y-axis, and k_w is the spring constant for the wall interaction.

As fracturing is not accounted for in linear elasticity theory, we have simulated its effects through the irreversible removal of a bond if the stress in the bond exceeds a maximum threshold value (σ^c), corresponding to the material strength. The material strength is assumed to be homogeneous on large scales, but to fluctuate around average values on the scale of individual particles. The variations correspond to variations in micro-crack densities and lengths, and other defects and variations which are always present in disordered materials. This local heterogeneity is described by a distribution of breaking thresholds, which corresponds to a distribution of the tensile strength of the material at a particular scale given by the scale of the elements. It can be demonstrated (Walmann *et al.* 1996; Malthe-Sørenssen *et al.* 1998*a*, *b*) that a normal distribution of breaking thresholds in this model reproduces fracture patterns observed in laboratory experiments and field studies. The average value of the breaking threshold may be related to the stress intensity factor (Flekkøy *et al.* 2002). The material behaviour can be tuned from a brittle material for narrow distribution of breaking threshold, to a more ductile behaviour for a wider distribution. We have extensive experience from simulating geological systems using this

model, and this experience was used in selecting realistic distributions of breaking thresholds. Typical values for the breaking threshold correspond to breaking strains $\varepsilon^c = 2 \times 10^{-3}$ to 2×10^{-2} (Fyfe *et al.* 1978). A value corresponding to a strain of 2×10^{-3} has been used in the simulations presented here.

The simulation procedure corresponds to a quasi-static driving mechanism of sill emplacement. Initially, the breaking strength of a short line is reduced by a factor of 10 in order to initialize sill emplacement in the horizontal direction. Sill injection is simulated by gradually increasing the pressure P_0 until a fracture occurs in the surrounding matrix. A bond is removed, and the fluid is allowed to fill the new volume. This reduces the pressure in the fluid according to linear relationship between change in fluid volume and pressure, with a magma compressibility corresponding to the elastic stiffness of the surrounding matrix. This computational scheme ensures that the sill propagates in small steps, and not as a runaway brittle fracture. A new equilibrium configuration is found for the elastic material for the pressure P_0. The procedure is then repeated by slowly increasing the pressure. Snapshots of the sill geometry and the stresses around it illustrate the growth of the sill and the emplacement process.

Modelling results

The coupled model is used to study the mechanisms for the formation of saucer-shaped sills in an undeformed, homogeneous basin. The basin is represented as an initially homogeneous material with an isotropic lithostatic stress. The sill was emplaced at a depth h corresponding to the level of neutral buoyancy for the magma. The width of the simulated region of the basin was 40 km, and typical values for the depth h were 1 to 5 km. Other material parameters were selected within the range of typical properties of a sedimentary basin: E = 2 GPa, $\Delta\rho$ = 0.25 Mg m^{-3}, $\varepsilon^c = 2 \times 10^{-3}$ (Atkinson 1984).

The developing geometry of the sill is illustrated in Figure 2 for a sill emplaced at at depth h = 1.8 km. Initially, the sill extends linearly, retaining its original orientation. In this regime, illustrated in Figure 2a, the sill is short compared to the thickness of the overburden. The shape of the sill and the stress field extending from the tips of the sill is approximately symmetrical, and the sill emplacement is not affected by the asymmetrical boundary conditions.

When the sill reaches a length of approximately the thickness of the overburden, the shape of the sill starts to become asymmetrical. This is illustrated by a plot of the position of the upper and lower sill surfaces shown in Figure 3. As a consequence, the stress in front of the sill tips becomes asymmetrical. Figure 2b illustrates the stress field immediately before the sill starts bending upwards.

The sill branches upwards due to the asymmetry of the stress field caused by the uplift of the overburden. This is illustrated in Figure 2c. Initially, the sill propagates steeply upwards; however, the ascent is limited by the reduction in pressure inside the sill, due to extension above its level of neutral buoyancy. Further development of the sill is shown in Figure 2d. We observe that the sill starts to develop an outer sill with lower inclination angle as the intrusion climbs further.

The formation of the saucer-shaped sill in the initially homogeneous basin can therefore be explained as an effect of an asymmetrical stress field generated by the sill intrusion itself and by the elastic interaction of the sill intrusion with the surrounding matrix. We have performed a series of simulations at various emplacement depths. A plot of the width of the horizontal part of the sill, w, as a function of the intrusion depth, h, is shown in Figure 4. The extent of the flat region of the sill, w, increases with depth due to increasing overburden. This observation is consistent with the cross-over from sill- to laccolith-like behaviour discussed by Johnson & Pollard (1973).

Discussion

Saucer-shaped sill complexes are frequently observed in unstructured sedimentary basins. The saucer-shaped sheet intrusions generally have a flat, circular central region, terminated at climbing sheet segments that cross-cut the sediments. Several saucers can be emplaced close to each other, interpenetrating and generating a complex interconnected pattern of sills.

Saucer-shaped sills are one of the most common structures observed in Karoo Basin, South Africa. This largely undeformed foreland basin is infilled with clastic sediments, which accumulated from the Late Carboniferous (310 Ma) (Vissner 1997) through the Mid-Jurassic (185 Ma) (Catuneaunu 1998). Voluminous extrusive and intrusive complexes were emplaced in the Karoo Basin at *c.* 183 Ma (Duncan *et al.* 1997).

The saucer-shaped sills control to a large extent the geomorphology of the landscape (Du Toit 1920; Chevallier & Woodford 1999). Figure 5a shows a sketch of the typical morphology of a ring structure. The Golden Valley (Fig. 5b) near

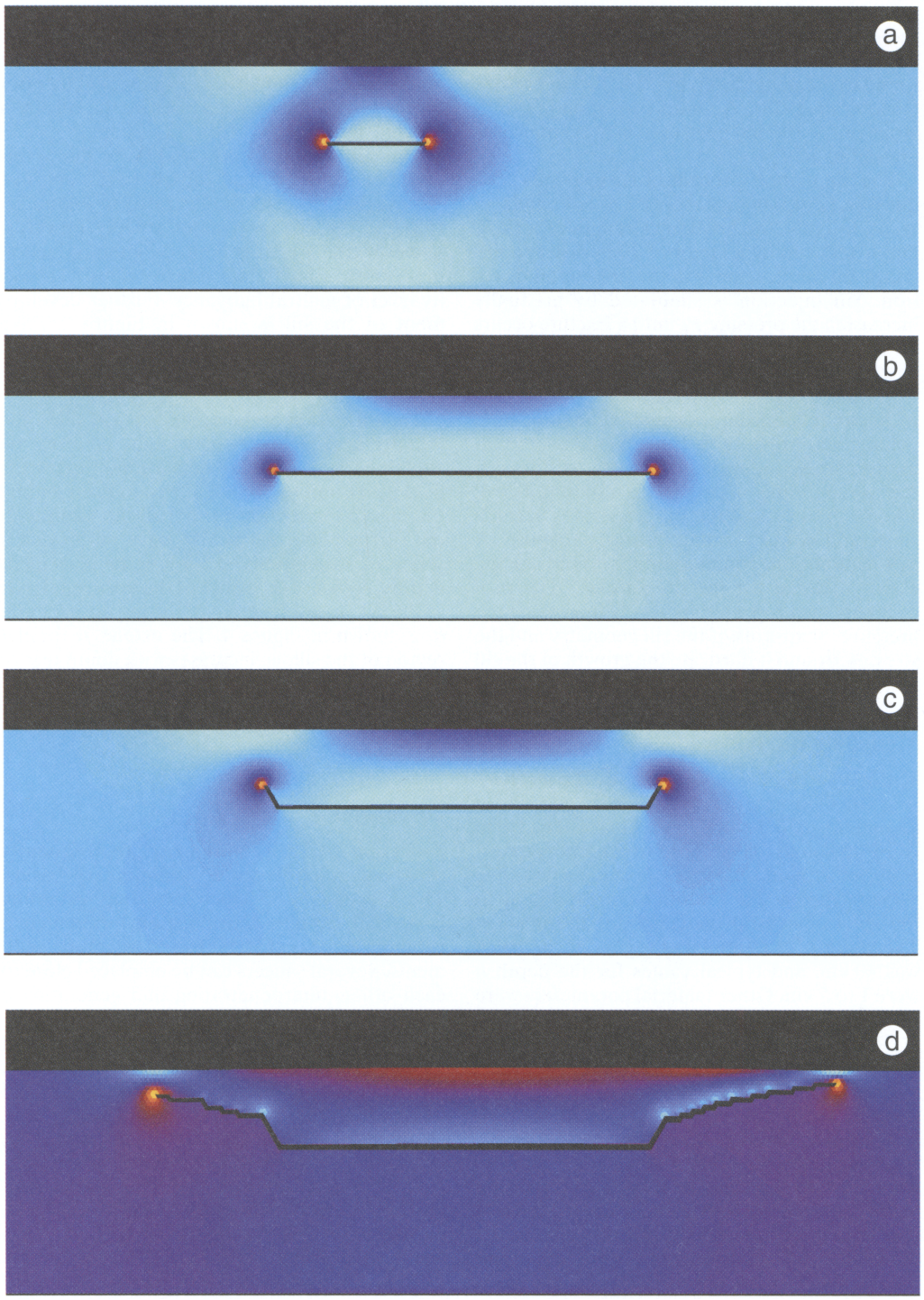

Fig. 2. Snapshots from a simulation of sill emplacement in a 40-km wide model. Only the central 20 km of the model is shown in the pictures. Figures (a) to (d) are snapshots showing various stages in the same simulation. The sill was emplaced at a depth of 1.8 km. The sill initially propagates horizontally, ((b) and (a)) but deflects upwards as the effect of the uplift of the overburden becomes important ((c) and (d)).

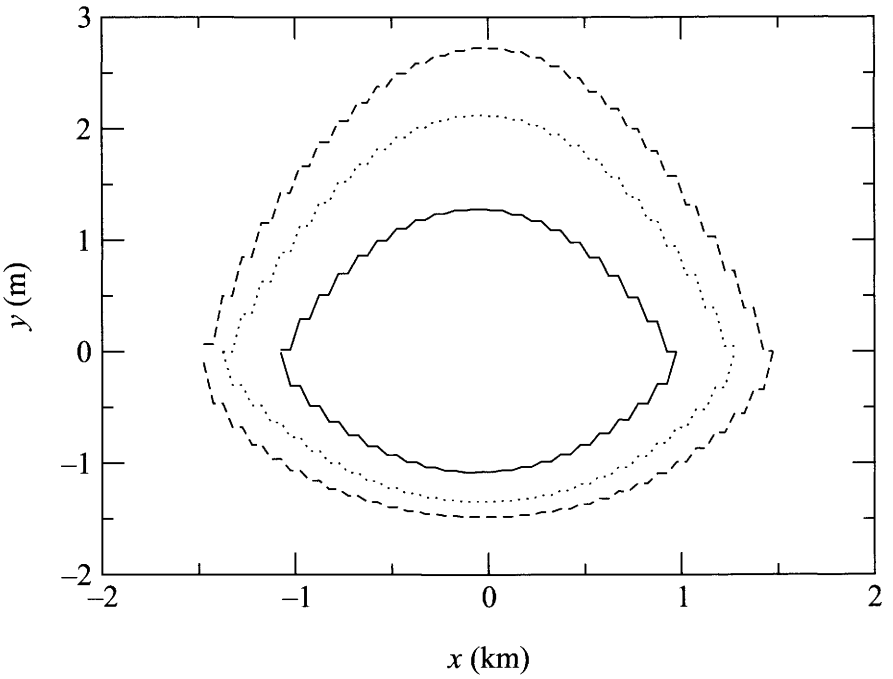

Fig. 3. The vertical position, y, of the top and bottom surfaces of the sill as a function of the spatial position along the sill, x, for several stages in the development of the sill. The shape of the sill becomes asymmetrical when it reaches a length approximately equal to the thickness of the overburden (1.8 km).

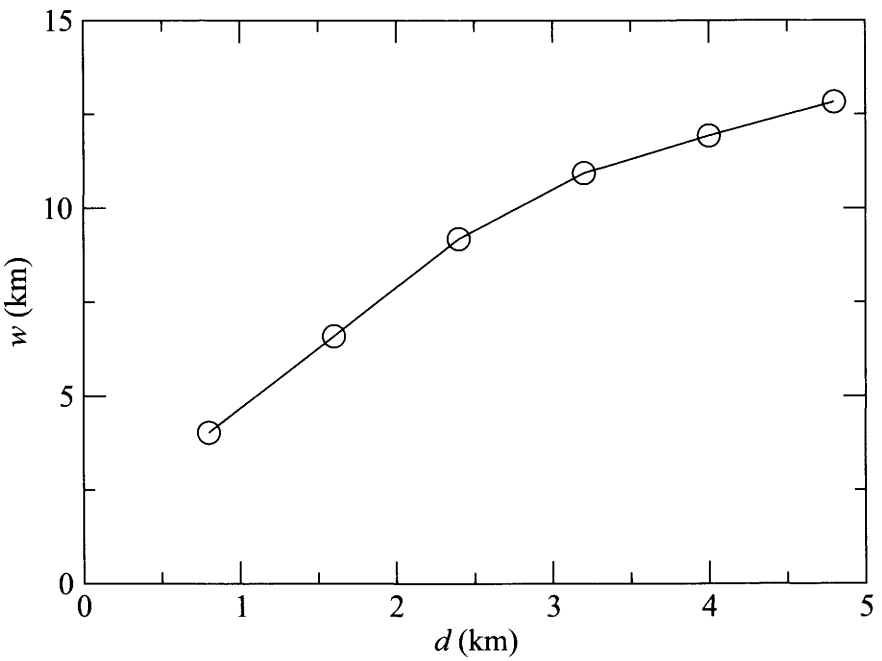

Fig. 4. The spatial extent, w, of the approximately horizontal part of the saucer-shaped sill as a function of emplacement depth, h, for simulations in a 40-km wide basin.

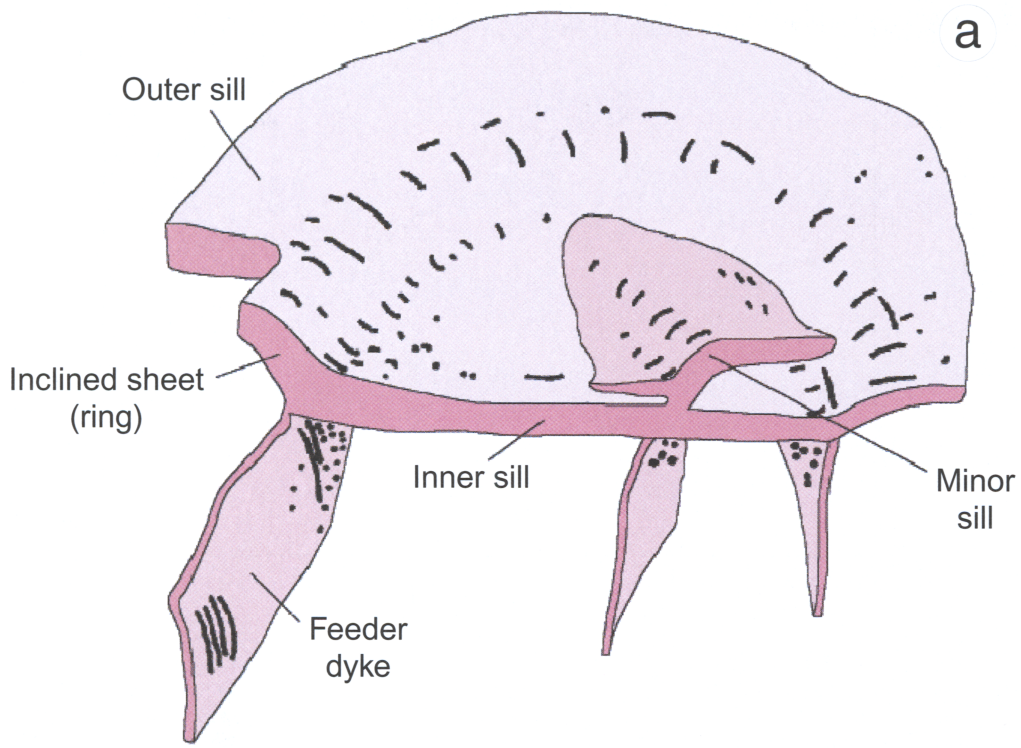

Fig. 5. (**a**) Sketch of the morphology of saucer-shaped sills and ring complexes in the Karoo Basin (after Chevallier & Woodford 1999). (**b**) Mosaic of aerial photographs of the Golden Valley sill. The Golden Valley is a classic saucer-shaped intrusion with a flat-lying central part and steep flanks. The saucer is 19 km by 10 km, with up to 350 m of elevation difference. (**c**) A photo of the Golden Valley sill seen from the outer southern part of the valley. Note that the inclined segments are formed by transgressive dolerites, and that the sedimentary sequence is approximately horizontal.

Queenstown is a large erosional basin defined by a saucer-shaped dolerite intrusion. The inclined rims are exposed as topographical highs that form an elliptical outcrop easily recognized on maps and aerial photographs. On the ground, the transgressive segments of the sill can clearly be seen to cross-cut the dominantly horizontally layered sedimentary strata (Fig. 5c). Similar saucer-shaped sill complexes are found regionally in the upper and middle parts of the Karoo Basin, whereas the sills in the lowermost sequences are dominantly subhorizontal.

Saucer-shaped sill intrusions are also commonly observed on volcanic rifted margins. Continental breakup between Greenland and Eurasia near the Palaeocene–Eocene transition was associated with voluminous extrusive and intrusive volcanism (Berndt *et al.* 2000). We have recently mapped the distribution of intrusions on more than 150 000 km of 2D seismic profiles and on 3D seismic data in the Vøring and Møre basins. The style of sill complexes clearly varies, with saucer-shaped intrusions dominating the undeformed basin segments.

The Gleipne Saddle in the outer Vøring Basin is located in a basin province with little pre- and post-magmatic structuring. Figure 6 shows a 3D image of a saucer-shaped high-amplitude seismic reflection interpreted as a sill intrusion. The size and geometry of this event is very similar to the geometry of the Golden Valley sill in the Karoo Basin (Fig. 5).

Saucer-shaped sills are also observed on the NW Australian shelf, e.g. on the Exmouth Plateau (Fig. 7). Here, the magmatism is associated with continental breakup between Australia and Greater India during the Valanginian (Symonds *et al.* 1998). A saucer-shaped sill intrusion can clearly be seen cross-cutting Triassic strata, locally causing deformation of the

Fig. 5. *continued.*

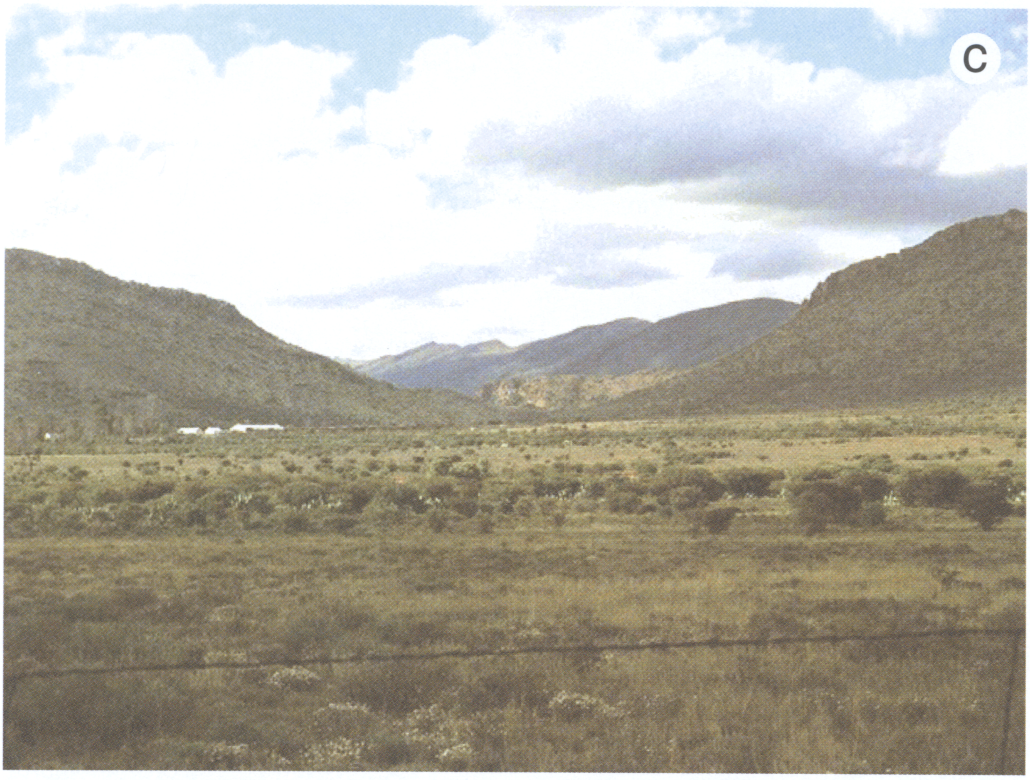

Fig. 5. *continued.*

overburden sediments (magma-tectonism) (Fig. 7).

Field and seismic data from mainly undeformed volcanic basin segments suggest that the saucer-shaped geometry is a fundamental shape for sheet intrusions. The coupled model illustrates a physically plausible mechanism for the formation of saucer-shaped sills in homogeneous basins. Previously, the idea that the uplift of the overburden could lead to the formation of dykes leading upwards from the sill tips has been discussed and illustrated by laboratory experiments (Pollard & Johnson 1973). An alternative explanation is that the sill follows the surface of neutral buoyancy, and that this surface is shaped as a saucer (Bradley 1965). While saucer-shaped isostress surfaces may exist in some basin geometries, and may indeed be quite common on larger scales in saucer-shaped basins, the explanation of Bradley (1965) is not relevant for the formation of saucer-shaped sills in unstructured basins, because this explanation relies on the sill following a pre-existing structure in the form of a saucer-shaped density profile, which, in general, would not be present in unstructured basins.

Our model demonstrates in a self-consistent framework that sufficiently large sills emplaced into consolidated, elastic materials, should develop into saucer-shaped geometries. Shallow sills intruding into unconsolidated sediments will not produce the long-range stress fields necessary for the formation of saucers, and we therefore expect sills to be disordered and more similar to lava flows at this scale. The model also explains why deeper sills are mainly layer-parallel: these sills are not long enough to start curving upwards (Fig. 4).

While the model is strictly two dimensional, the fundamental mechanism presented here is equally valid in three dimensions. Boundary effects play a more important role in two-dimensional elasticity, because perturbations decay logarithmically in two dimensions. Also, the effective elastic stiffness of the overburden in the two-dimensional model is expected to be significantly lower than in a cylindrical symmetrical three-dimensional model. The functional

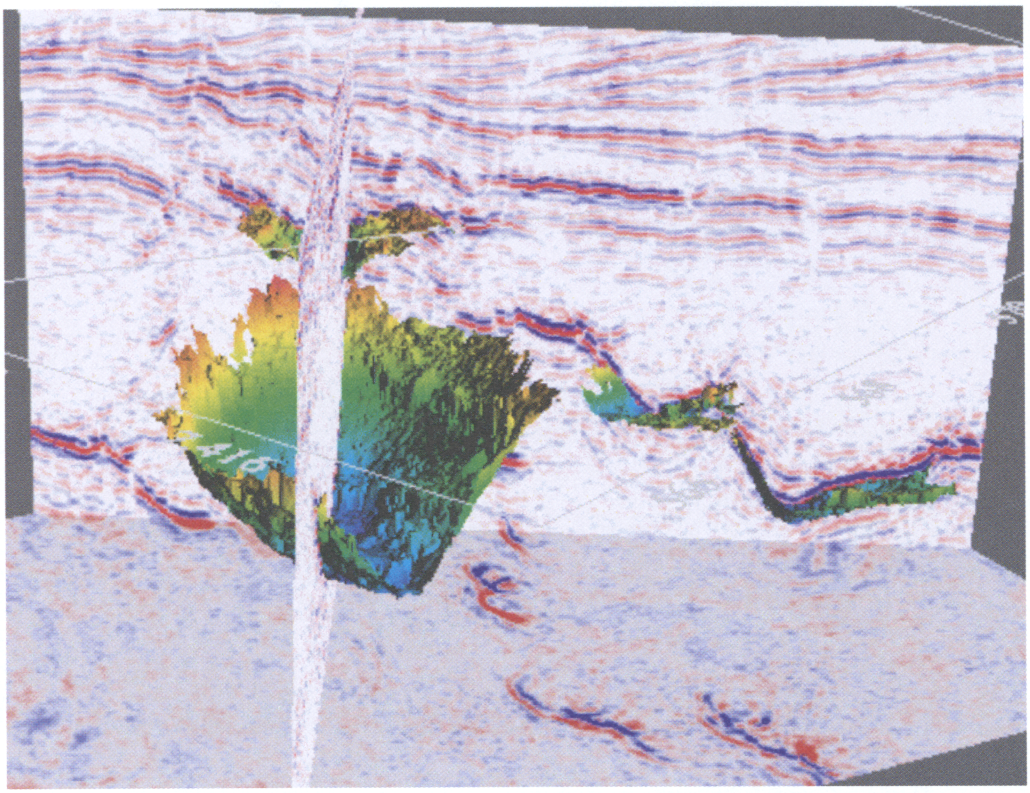

Fig. 6. 3D visualization of a saucer-shaped high-amplitude reflection on the Gleipne Saddle, Outer Vøring Basin. The event is interpreted as a sill reflection, with a geometry and size similar to the Golden Valley sill. The high-amplitude event is auto-tracked and plotted using the VoxelVision software. The main saucer is 3 km by 4 km, with approximately 500 m of elevation difference.

form of the relation between saucer extent and emplacement depth therefore cannot be compared directly with field and seismic data. However, the qualitative dependence is expected to be correctly represented.

Conclusions

We have developed a new, coupled numerical model for emplacement of magma in sedimentary basins. The host rock is modelled as an elastic material using a discrete element method where fracturing is accompanied by removal of elements. The magma is modelled as a non-viscous fluid.

Numerical modelling of sill emplacement in the simplest scenario – non-viscous magma emplaced in an undeformed, homogeneous basin – demonstrates that saucer-shaped sills are formed spontaneously and represent a fundamental shape. The saucer-shaped structure is generated due to interactions between the sill and the overburden. The emplacement process introduces stress heterogeneities in the basin, which subsequently influence the geometry of the emplaced sill.

The transgressive nature of sill emplacement is a fundamental effect that should be taken into consideration when studying sill emplacement. The saucer shape is a fundamental shape in shallow sills: our model indicates that sills will be flat unless their extent exceeds the depth by a factor of two to three, depending on details of the material properties of the overburden.

There is good agreement between the modelling results and observational data from seismic interpretation of the Vøring and Møre basins, offshore Mid-Norway, and on the NW Australian Shelf, and field studies in the Karoo Basin, South Africa. The model provides a unifying explanation for the observation of saucer-shaped intrusions in shallow to intermediate

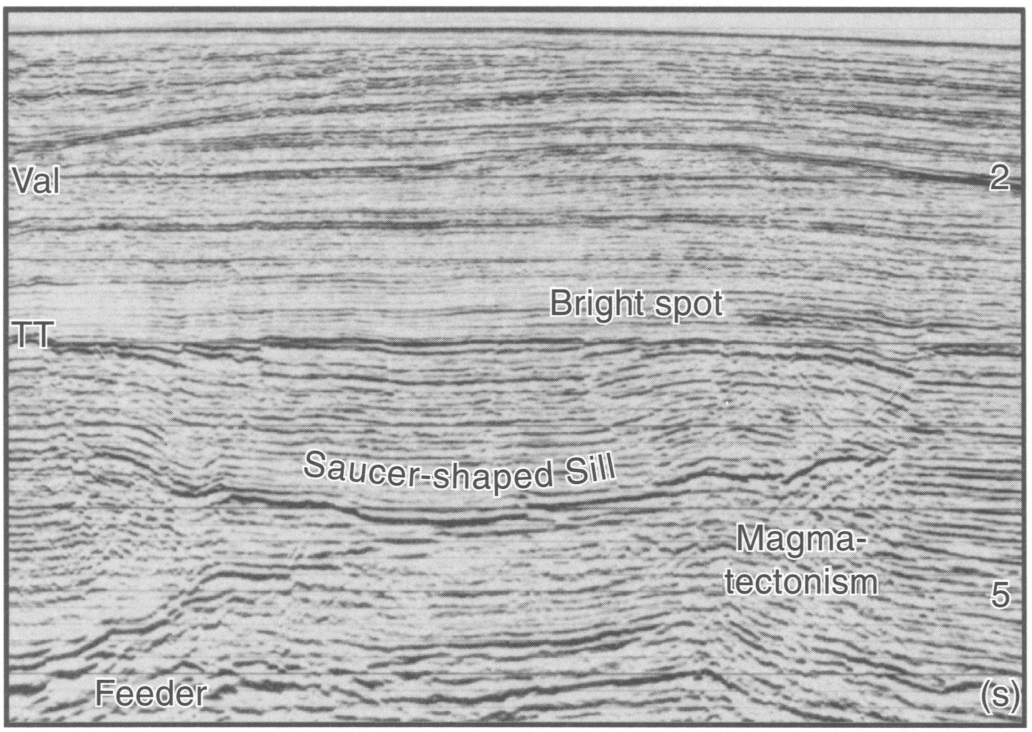

Fig. 7. Saucer-shaped high-amplitude event interpreted as a magmatic sill cross-cutting Triassic sedimentary strata on the Exmouth Plateau, Australian NW Shelf. Modified from Symmond *et al.* (1998). The width of the saucer is 27 km.

emplacement depths, and provides a framework in which more complicated sill emplacement geometries and more complicated emplacement dynamics can be studied.

We gratefully acknowledge access to seismic data from TGS–NOPEC, and financial support from the sponsors of the 'Petroleum Implications of Sill Intrusion' project, and the Norwegian Research Council. L. Chevallier, Council of Geoscience, South Africa, and G. Marsh, Rhodes University, South Africa have provided valuable information and fieldwork guidance. The VoxelVision interpretation was done by S. Johansen of the Bridge Group.

References

ALLEN, D.M.D.G. 1954. *Relaxation Methods*. McGraw-Hill, New York.

ATKINSON, B.K. 1984. Subcritical crack growth in geological materials. *Journal of Geophysical Research*, **89**, 4077–4114.

BERNDT, C., SKOGLY, O.P., PLANKE, S., ELDHOLM, O. & MJELDE, R. 2000. High-velocity breakup-related sills in the Vøring Basin off Norway. *Journal of Geophysical Research*, **105**, 28 443–28 454.

BRADLEY, J. 1965. Intrusion of major dolerite sills. *Transactions of the Royal Society of New Zealand, Geology*, **3**, 27–55.

CATUNEAUNU, O., HANCOX, P.J. & RUBIDGE, B.S. 1998. Reciprocal flexural behavior and contrasting stratigraphies: a new basin development model of the Karoo retroarc foreland system, South Africa. *Basin Research*, **10**, 417–439.

CHEVALLIER, L. & WOODFORD, A. 1999. Morphotectonics and mechanism of emplacement of the dolerite rings and sills of the western Karoo, South Africa. *South African Journal of Geology*, **102**, 43–54.

CORRY, C.E. 1988. Laccoliths: mechanisms of emplacement and growth. *Geological Society of America, Special Papers*, **220**, 1–110.

DUNCAN, R.A., HOOPER, P.R., REHACEK, J., MARSH, J.S. & DUNCAN, A.R. 1997. The timing and duration of the Karoo igneous event, southern Gondwana. *Journal of Geophysical Research*, **102**, 18 127–18 138.

DU TOIT, A.I. 1920. The Karoo dolerites. *Transactions of the Geological Society South Africa*, **33**, 1–42.

FLEKKØY, E.G., MALTHE-SØRENSSEN, A. & JAMTVEIT, B. 2002. Modeling hydrofracture. *Journal of Geophysical Research*, **107**, 10 259–10 272.

FRANCIS, E.H. 1982. Magma and sediment – I: emplacement mechanism of late Carboniferous

tholeiite sills in the northern Britain. *Journal of the Geological Society of London*, **139**, 1–20.

FYFE, W.S., PRICE, N. & THOMPSON, A.V. 1978. *Fluids in the Earth's crust*. Elsevier Science, New York.

GILBERT, G.K. 1877. *Geology of the Henry Mountains, in the U.S.* Geographical and Geological Survey of the Rocky Mountain Region, U.S. Government Printing Office, Washington, D.C., USA.

JAMTVEIT, B., AUSTRHEIM, H. & MALTHE-SØRENSSEN, A. 2000. Accelerated hydration of the Earth's deep crust induced by stress perturbations. *Nature*, **107**, 10 259–10 272.

JOHNSON, A.M. & POLLARD, D.D. 1973. Mechanics of growth of some laccolithic intrusions in the Henry Mountains, Utah, 1. *Tectonophysics*, **18**, 261–309.

KHAZAN, Y.M. & FIALKO, Y.A. 1995. Fracture criteria at the tip of fluid-driven cracks in the earth. *Geophysical Research Letters*, **22**, 2541–2544.

LISTER, J.R. & KERR, R.C. 1991. Fluid-mechanics models of crack propagation and their application to magma transport in dykes. *Journal of Geophysical Research*, **96**, 10 049–10 077.

MALTHE-SØRENSSEN, A., WALMANN, T., FEDER, J., JØSSANG, T., MEAKIN, P. & HARDY, H.H. 1998*a*. Simulation of extensional clay fractures. *Physical Review E*, **58**, 5548–5564.

MALTHE-SØRENSSEN, A., WALMANN, T., JAMTVEIT, B., FEDER, J. & JØSSANG, T. 1998*b*. Modeling and characterization of fracture patterns in the Vatnajökull glacier. *Geology*, **26**, 931–934.

MONETTE, L. & ANDERSON, M.P. 1994. Elastic and fracture properties of the 2-dimensional triangular and square lattices. *Modelling and Simulation in: Materials Science and Engineering*, **2**, 53–73.

POLLARD, D.D. & JOHNSON, A.M. 1973. Mechanics of growth of some laccolithic intrusions in the Henry Mountains, Utah, 2. *Tectonophysics*, **18**, 311–354.

POLLARD, D.D., MULLER, O.H. & DOCKSTADER, D.R. 1975. The form and growth of fingered sheet intrusions. *Geological Society of America Bulletin*, **86**, 351–363.

RUBIN, A.M. 1993. Tensile fracture of rock at high confining pressure: implications for dike propagation. *Journal of Geophysical Research*, **98**, 15 919–15 935.

RUBIN, A.M. 1995. Propagation of magma-filled cracks. *Annual Review, Earth Planetary Sciences*, **23**, 287–336.

SCHUTTER, S.R. 2003. *Hydrocarbon Occurrence and Exploration in and Around Igneous Rocks*. Geological Society, London, Special Publications, **214**.

SKOGSEID, J., PEDERSEN, T., ELDHOLM, O. & LARSEN, B. 1992. Tectonism and magmatism during NE Atlantic continental break-up: the Vøring margin. *Geological Society, London, Special Publications*, **68**, 305–320.

SMALLWOOD, J. & MARESH, J. 2002. *The Properties, Morphology and Distribution of Igneous Sills: Modelling, Borehole Data and 3d Seismic from the Faroe–Shetland Area*. Geological Society, London, Special Publications, **197**.

SYMONDS, P.A., PLANKE, S., FREY, Ø. & SKOGSEID, J. 1998. Volcanic development of the Western Australian continental margin and its implications for basin development. *In*: PURCELL, P.G. & PURCELL, R.R. (eds) *The Sedimentary Basins of Western Australia 2, Proceedings of the Petroleum Exploration Society of Australia, Symposium, Oxford*, Petroleum Exploration Society of Australia, Perth, Australia, 33–54.

VISSNER, J.N.J. 1997. Geography and climatology of the Late Carboniferous to Jurassic Karoo Basin in the south-western Gondwana. *South African Journal of Geology*, **100**, 233–236.

WALMANN, T., MALTHE-SØRENSSEN, A., FEDER, J., JØSSANG, T., MEAKIN, P. & HARDY, H.H. 1996. Scaling relations for the lengths and widths of fractures. *Physical Review Letters*, **77**, 5393–5396.

Table 1. *List of symbols*

ϕ	Porosity of particle packing	i	Particle index
ε^c	Critical strain – strain at which a spring breaks	$k_{i,j}, k$	Spring constant
ρ_m	Matrix mass density	k_w	Spring constant for wall interaction
ρ_i	Particle mass density	$k'_{i,j}$	Non-dimensional spring constant
ρ_s	Magma mass density	$l_{i,j}$	Equilibrium length for spring from i to j
$\Delta\rho$	Density difference between magma and matrix	l	Physical length, typical equilibrium length
σ'_{ij}	Non-dimensional stress tensor	m	Mass of particle
σ_{ij}	Stress tensor	P	Magma pressure at height y
σ^c	Critical stress – stress at which a spring breaks	P_0	Magma pressure at point of injection
A_i	Contact area between magma and particle	r_i	Radius of particle i
E	Young's modulus of matrix	$\boldsymbol{u}_{i,j}$	Unit vector from node i to node j
E_0	Young's modulus of a spring		Surface normal for the sill–sediment interface
	Interparticle force on particle i	$\boldsymbol{u}_y$	Unit vector along the y-axis
	Force on particle i due to gravity	w	The width of the horizontal part of the sill
	Magma-pressure force on particle i	w_z	Thickness of the two-dimensional sample
	Net force on particle i	$\boldsymbol{x}_j$	Position of node j
g	Acceleration of gravity	$\boldsymbol{x}'$	Non-dimensional spatial position
h	Sill emplacement depth	y_w	Position of vertical wall, i.e. elastic boundary